Journal of ELECTRONIC MATERIALS, Vol. 44, No. 11, 2015
DOI: 10.1007/s11664-015-3982-3

Effect of Process and Service Conditions on TLP-Bonded Components with (Ag,Ni–)Sn Interlayer Combinations

ADRIAN LIS[1] and CHRISTIAN LEINENBACH[1,2]

1.—Empa, Swiss Federal Laboratories for Materials Science and Technology, Laboratory for Joining Technologies and Corrosion, Ueberlandstrasse 129, 8600 Dübendorf, Switzerland. 2.—e-mail: christian.leinenbach@empa.ch

Transient liquid phase (TLP) bonding of Cu substrates was conducted with interlayer systems with the stacking sequences Ag–Sn–Ag (samples A), Ni–Sn–Ni (samples B), and combined Ag–Sn–Ni (samples C). Because of the low mismatch of the coefficients of thermal expansion, characteristics of the TLP process and mechanical and thermal behavior of TLP-bonded samples could be investigated without interference from thermally induced residual stresses. An ideal process temperature of 300°C, at which the number of pores was lowest, was identified for all three layer systems. It was verified experimentally that formation of pores resulted from volume contraction during isothermal solidification of liquid Sn into intermetallic compounds (IMC). Temperature and interlayer-dependent growth characteristics of IMC accounted for the increasing size and number of defects with increasing process temperature and for different defect positions. The shear strength was measured to be 60.4 MPa, 27.4 MPa, and 40.7 MPa for samples A, B, and C, respectively, and ductile fracture features were observed for Ag_3Sn IMC compared with the purely brittle behavior of Ni_3Sn_4 IMC. Excellent thermal stability for all three layer systems was confirmed during long-term annealing at 200°C for up to 1200 h, whereas at 300°C the microstructure was driven toward Ag–Sn solid solution, accompanied by Cu diffusion from the substrate along grain boundaries and Cu_3Sn IMC formation (A), and toward Ni-rich IMC phases (B). Combined IMC interlayers (C) tended to be transformed into Ni-based IMC when held at 300°C; intermixing into $(Ni,Cu)_3Sn$ was accompanied by pore formation.

Key words: TLP bonding, microstructure, defect formation, shear strength, annealing

INTRODUCTION

Power module packaging faces demanding challenges because of harsh restrictions on Pb-based solder alloys and the increasing tendency to miniaturize devices by introducing SiC technology. Replacement of Si semiconductors has the potential to result in greater efficiency, because SiC is much more temperature-resistant, so power modules can theoretically operate at higher temperatures and active cooling systems or heat sinks can be reduced or even avoided.[1,2] In this context, transient liquid phase (TLP) bonding has been identified as a promising low-temperature joining technique which satisfies the above mentioned demands of chip packaging.

Low-temperature TLP bonding is achieved by placing a sandwiched interlayer system consisting of a high-melting-point material, i.e. Cu, Ni, Ag, or Au, and a low-melting-point material, i.e. Sn or In, between the two components to be joined. After melting of the interlayer, interfacial formation of intermetallic compounds (IMC) starts and isothermal solidification of the connection proceeds until

(Received March 12, 2015; accepted August 10, 2015; published online August 28, 2015)

the liquid metal is fully consumed. This diffusion-controlled mechanism leads to the exceptional feature of TLP bonding that the remelting temperature of the joint is higher than the process temperature.[3]

However, before TLP bonding can be reliably implemented in applications, fundamental research is required to enable understanding and control of the joining process and for determination of the durability and limitations during operating conditions. Many researchers have investigated the growth kinetics, diffusion mechanisms, and morphological characteristics of formation of IMC from different layer systems, e.g. Cu–Sn,[4–7] Ni–Sn,[4,8–12] Ag–Sn,[13–18] or In-based systems.[19–23] Schaefer et al.[6] developed a model in which grain boundary (GB) diffusion was identified as the factor responsible for the observed $t^{1/3}$ growth kinetics of the Cu–Sn IMC layer with scallop-like morphology. Li et al.[14] used sandwiched Ag–Sn–Ag structures to determine the kinetics of scallop-like Ag_3Sn IMC growth, and confirmed the $t^{1/3}$-dependence for temperatures of 260°C, 300°C, and 340°C and holding times from 5 min to 475 min. Gur and Bamberger[10] identified a microstructural transition zone (MTZ) which was explained by the simultaneous and opposite growth of coarse-grained Ni_3Sn_4 IMC toward the Sn side and fine-grained Ni_3Sn_4 toward the Ni substrate. The IMC scallops observed at 500°C were shown to transform into elongated faceted grains compared with reaction at lower temperatures of 400°C and 350°C. In a different approach, Görlich et al.[19] used near-isothermal experimental conditions (250°C) from 30 s to 7 days of holding time and observed that Ni_3Sn_4 IMC growth kinetics were best fitted by a cubic growth law for periods up to 3 min but followed a parabolic function for longer holding times. Needle-like Ni_3Sn_4 IMC at the Ni–Sn interface and detached polygonal IMC crystals were observed, in good agreement to the work of Bader et al.[8] These fundamental studies aided understanding of the effect of such conditions as temperature, time, and heating rate, and the grain structure and chemical composition of the layers on IMC growth behavior during TLP bonding.

Effort has also been devoted to characterization of TLP bonded chips to metallic substrate materials when a high mismatch between the coefficients of thermal expansion (CTE) strongly affects the microstructural,[24–26] mechanical,[27–29] or electrical properties[30] after processing, annealing, or thermal cycling.

However, the characteristics of the TLP process and the thermal stability of TLP bonded components without or with a negligible CTE mismatch have hardly been investigated. Bosco et al.[31] TLP bonded Cu substrates with coated Sn interlayers at 550°C and derived a model for defect formation which predicted that a minimum thickness of Sn is required to minimize defects. This condition ensures that a continuous Sn layer is left after heating and the corresponding solid-state formation of Cu–Sn IMC before the melting point of Sn is exceeded and the solid–liquid reaction starts. While useful, the proposed model seems to be valid only for coated interlayers and the process temperature investigated is much too high for chip packaging. In follow-up work,[32] they observed that heat treatment for 30 min at 550°C improved the initial bending strength of Cu–Sn TLP bonded rod specimens from 300 MPa to 400 MPa, because of a change in microstructure from pure IMC to a mixture of IMC and Cu–Sn solid solution. Gollas et al.[33] used TLP-bonded Cu substrates with Ag–Sn/In–Ag interlayers for high-temperature *in situ* x-ray diffraction (XRD) measurements during annealing at 320°C. They tracked the transformation of Ag_3Sn into Ag_5Sn after 40 min and subsequently into Ag–Sn solid solution after 480 min of holding time. Chung et al.[34] proposed the use of Sn2.4Ag solder instead of pure Sn to join Ni-coated substrates. Voids within the Ni_3Sn_4 IMC layer were filled by Ag_3Sn IMC in long-term solid-state reactions. Similarly, a patent by Chang et al.[35] claims elimination of voids within the IMC layer as a result of formation of a dual-phase IMC layer by applying interlayers between two substrates with different metallization.

In this work, three different interlayer systems, Ag–Sn–Ag, Ni–Sn–Ni, and combined layers of Ag–Sn–Ni, were investigated by use of the same methodology. Microstructural analysis of TLP-bonded Cu specimens was performed to find the optimum process conditions for chip packaging (T_{max} = 350°C) from the perspective of both process kinetics and the appearance of joining defects. General and interlayer-dependent mechanisms for defect formation, mechanical shear strength, and failure behavior are of interest for TLP-bonded samples with the three interlayer systems. Near-service conditions on TLP joints were simulated by annealing experiments at 200°C and 300°C while microstructural changes were monitored over time.

EXPERIMENTAL

Two Cu plates with the dimensions 110 mm × 60 mm × 4 mm were electroplated with 14 μm Ag and with 17 μm Ni, respectively. After coating, both plates were cut into smaller 5 mm × 5 mm × 4 mm samples by electrical discharge machining (EDM) and the sharp sample edges were chamfered at an angle of 45°, which reduced the effective bonding area to 20.25 mm^2 (4.5 mm × 4.5 mm). Sn foil of thickness 8 μm and purity 99.75% was used (Goodfellow Cambridge), to avoid solid-state reactions during heating which occur for coated interlayers, as discussed elsewhere.[31] The surface and bulk quality of the coated layers (after cutting and degreasing) and the Sn foil (as-delivered) were analyzed by x-ray photoelectron spectroscopy (XPS). A small amount of sulfate was found on the Ag coating because of contact with the

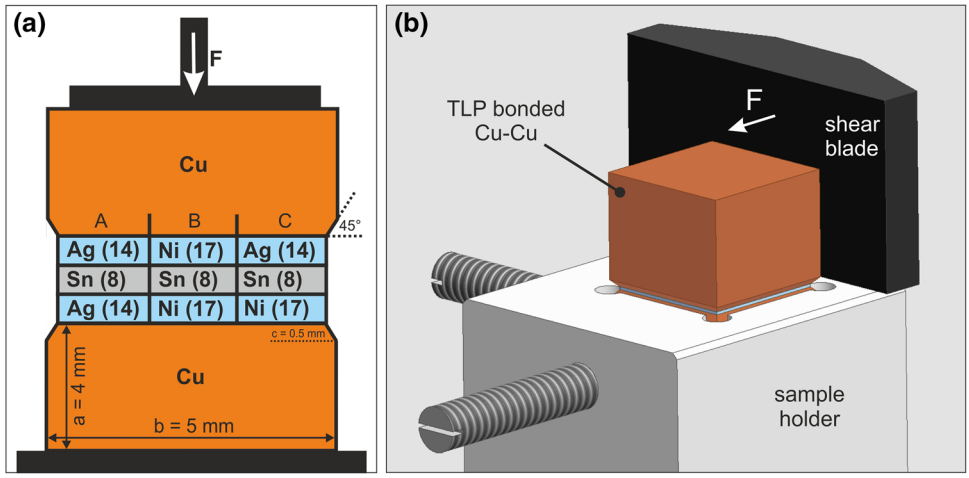

Fig. 1. (a) Schematic diagram of assembly of coated Cu substrates and Sn foil for TLP bonding (all values in brackets are in μm); (b) shear test set up for TLP-bonded Cu substrates.

dielectric medium during EDM; no residues were observed on the surface of the Ni coating. The surface of the Sn foil was contaminated with reaction products containing S, P, and Cr; an oxide layer of thickness 10 nm was also detected. To remove contaminants and oxides, Ag-coated Cu substrates and the Sn foil were dipped for seconds in HNO_3 (5 vol.%) and HCl (10 vol.%), respectively. Substrates and foil were assembled in accordance with Fig. 1a to perform TLP bonding with Ag–Sn–Ag (samples A), Ni–Sn–Ni (samples B), and Ag–Sn–Ni (samples C) interlayer combinations.

Investigations on combined interlayers are of interest for technical applications in which (different) as-delivered coatings may be used for TLP bonding instead of depositing additional layers and when the approaches discussed in Refs. 34 and 35 are applied. All joining experiments were conducted in a tube furnace system under an argon 6.0 shielding gas atmosphere while applying a bonding pressure of 0.3 MPa. A heating rate of 15°/min was selected but slow cooling of approximately 2°/min was used to minimize thermal gradients within the samples. The process temperature varied among 260°C, 300°C, and 350°C and the isothermal holding time was adjusted in accordance with the IMC growth kinetics investigated in our previous work.[15,36] The rate of consumption of Sn, $z_{Sn,con}$, was determined as a function of temperature and time according to:

$$z_{Sn,con}(T,t) = \left[\left(\frac{\varphi}{\varphi+1}\right)\sqrt{k_0 \exp\left(\frac{-Q}{RT}\right)\cdot t}\right] = \left(\frac{\varphi}{\varphi+1}\right)\cdot z_{IMC}(T,t) \quad (1)$$

with

$$\varphi = \frac{Y}{X}\cdot\frac{M(Sn)/\rho(Sn)}{M(B)/\rho(B)} \quad (2)$$

where φ is the transformation factor which describes how much Sn (in volume or thickness) is consumed by formation of an IMC layer z_{IMC} of defined thickness. M is the molar mass, ρ is the density of Sn and base material B (Ag or Ni). X and Y are the stoichiometric atomic ratios of the forming IMC, e.g. X is 3 and Y is 4 for Ni_3Sn_4 IMC. R is the universal gas constant, t is the time, and T is the process temperature in Kelvin. The activation energy Q with identical electroplated coatings was derived as 30.6 kJ/mol for Ag_3Sn IMC growth[15] and 43.3 kJ/mol for Ni_3Sn_4 IMC growth;[36] the proportionality constant k_0 was 4.6×10^{-7} cm^2/s for the Ag–Sn system and 4.93×10^{-7} cm^2/s for the Ni–Sn system. The holding time t for TLP bonding can be calculated by transforming Eq. 1 and inserting the holding temperature T and the required Sn consumption of 4 μm (at both base metal–Sn interfaces). Calculation resulted in holding times of 80 min at 260°C, 60 min at 300°C, and 45 min at 350°C for the three interlayer systems to fully consume the liquid Sn phase. These temperatures were selected because joining processes in high-power modules are limited to 350°C, at which the semiconducting properties of Si and the consistency of polymeric insulators are not affected.

Cu was selected as substrate material to minimize thermally induced residual stresses after joining and to achieve rapid and homogeneous heating of the samples. After the TLP process, the samples were embedded in cold mounting resin and prepared metallographically by step-wise grinding and final polishing with silica suspension. The polished samples were subsequently treated by argon ion beam flat milling (Hitachi IM4000) to remove preparation artefacts, for example smearing between ductile interlayers. Microstructure was investigated by scanning electron microscopy (SEM; Hitachi S-3700 N) and energy-dispersive x-ray spectroscopy (EDS; EDAX Octane Pro). Mechanical

shear strength was investigated for samples from series A, B, and C which had been TLP bonded at 300°C, because of their small number of defects (shear test device by Walter and Bai). A sample holder, shown in Fig. 1b, was designed to guarantee ideal fixing and adjustment to a shear blade consisting of tungsten carbide (WC) and to apply the shear force F directly above the TLP joint. The mean shear strength was determined from 7 measurements for every sample type. Overlaying bending moments M on the joint during shear testing can be estimated for our set up by use of Eq. 3; the results are listed in Table I.

$$M = F \cdot \left(\frac{a-c}{2}\right) \quad (3)$$

Fractographic analysis by SEM and EDS was performed to determine failure mode and position. Furthermore, TLP-bonded samples A, B, and C with smallest number of defects, i.e. those joined at 300°C, were subjected to isothermal annealing at temperatures of 200°C and 300°C for up to 1200 h of holding time in an air furnace (Nabertherm). Microstructural changes during annealing were analyzed by SEM and EDS on cross sections, as described above.

RESULTS

TLP Bonding with Ag–Sn–Ag Interlayers

Phase Formation During TLP Bonding

TLP bonding on samples A with Ag–Sn–Ag interlayers was performed at 300°C and 350°C. At both temperatures, the process was interrupted after 1 min of dwell time to freeze an intermediate stage of Ag_3Sn IMC formation. At 300°C, small and randomly distributed IMC scallops can be observed in Fig. 2a; similar larger scallops with an averaged lateral grain size of 10 μm evolve when the temperature is increased to 350°C, as shown in Fig. 2b. Some of these large scallops already reach the opposite reaction front line after short holding time of 1 min. After full consumption of Sn, TLP joints produced at 350°C contain a large number of pores within the IMC layer (Fig. 2d) whereas a lower process temperature of 300°C leads to significant reduction of defect size and amount, as shown in Fig. 2b. EDS measurements revealed a higher concentration of Sn in the Ag layers after processing at 350°C than after processing at 300°C, i.e. approximately 4 at.% and approximately 2 at.%, respectively. Ag can be distinguished from the Ag_3Sn IMC by the different grain size; the Ag layers have a much finer grain structure compared with the sandwiched Ag_3Sn IMC layer between them. Shear tests were performed on samples TLP bonded at 300°C which contain significantly fewer defects. The measured values are summarized in Table I. The mean measured external shear force F_{mean} was 1222 ± 141 N; this corresponds to a mean shear strength, τ_{mean}, of 60.4 ± 7 MPa when the effective bonding area is considered. Pronounced shear marks, shown in Fig. 3a, were observed all over the fracture surface, indicating the force direction parallel to the joint. In a small volume at the end opposite to that of shear force introduction, plastic deformation marks were found, as shown in Fig. 3b. The tilt angle represents the force direction, and suggests a small fraction of tensile loading. This is most likely to be related to crack opening immediately before fracture so that the top substrate slightly tilts and the applied force no longer acts parallel to the joint. Only cohesive fracture within the Ag_3Sn IMC layer was observed.

Phase Formation During Annealing

Long-term annealing was performed on samples A bonded at a processing temperature of 300°C. After annealing at 200°C for 400 h, the concentration of Sn in the surrounding Ag layers increased to 4 at.% on average. After 1200 h, EDS measurements confirmed that 7 at.% Sn had dissolved in the Ag layers. According to the binary Ag–Sn phase diagram, the maximum solubility of Sn in the fcc Ag crystal lattice is approximately 10 at.% between 200°C and 400°C.

Changes in microstructure after isothermal annealing at 300°C for 400 h are shown in Fig. 4. Sn had dissolved in the Ag layers and reached its solid solution concentration of approximately 10 at.%. The Ag_3Sn and Ag layers still differ in grain size, as depicted in Fig. 4a. When the BSE phase contrast was strongly amplified, formation of an additional phase, i.e. Cu_3Sn, was revealed (Fig. 4b); it was equally distributed within the Ag_3Sn and Ag layers. The volume fraction of Cu_3Sn in the surrounding Ag

Table I. Summary of shear test results for samples A, B, and C

Sample	F_{mean} (N)	SD (force) (N)	σ_{mean} (MPa)	SD (stress) (MPa)	M_{mean} (Nm)	σ_{max} (MPa)	σ_{min} (MPa)
A Ag–Sn–Ag	1222	141	60.4	7	2.14	64.5	49.1
B Ni–Sn–Ni	554	130	27.4	6.4	0.97	33.3	19.5
C Ag–Sn–Ni	825	318	40.7	13.7	1.44	59.7	24.2

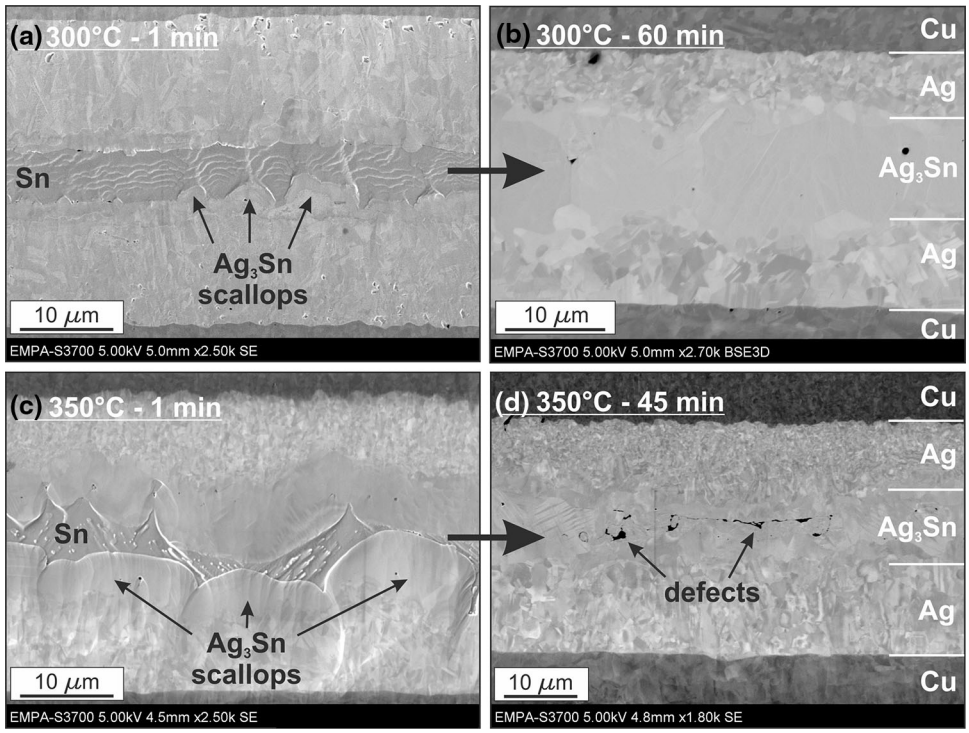

Fig. 2. TLP bonding of samples A at 300°C for (a) 1 min and (b) 60 min, and at 350°C for (c) 1 min and (d) 45 min.

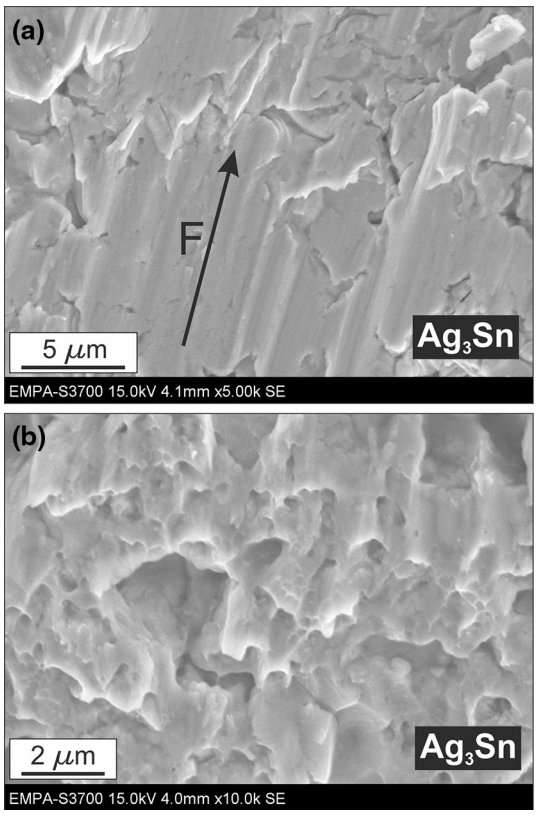

Fig. 3. Top view of fracture surface of samples A with (a) shear marks as the predominant feature and (b) dimples in a small area at the end opposite to that of shear force introduction.

and Ag_3Sn matrix was measured from the phase contrast in the binary image as 3.8 vol.%. Cu_3Sn IMC formation evolves along grain boundaries which leads to their elongated shape. Diffusion rates of Cu into both Ag and Ag_3Sn are sufficiently high at 300°C to cross the layered structure whereas at 200°C this effect was not observed.

Diffusion of Cu continues when annealing is continued for 1200 h; this results in the growth of existing Cu_3Sn particles and the nucleation of new Cu_3Sn particles. Figure 4c and d show the significant volumetric increase of Cu_3Sn fraction to 14.4 vol.%. The difference between the grain sizes of Ag and Ag_3Sn has vanished in Fig. 4c, and EDS measurements confirmed that the Cu_3Sn IMC particles are embedded in a matrix of Ag–Sn solid solution containing 10 at.% of Sn.

TLP Bonding with Ni–Sn–Ni Interlayers

Phase Formation During TLP Bonding

TLP bonding for series B was performed with Ni–Sn–Ni interlayers. TLP-bonded samples obtained at 260°C in Fig. 5a and at 300°C in Fig. 5b have similar microstructure. Characteristic defects form within the Ni_3Sn_4 IMC layer, with pores positioned at a more or less constant distance of 1 μm from the Ni–Ni_3Sn_4 interface, leading to the formation of two defect planes. Interestingly, no defects could be observed along the bond center line. However, if the process temperature is increased to 350°C, large

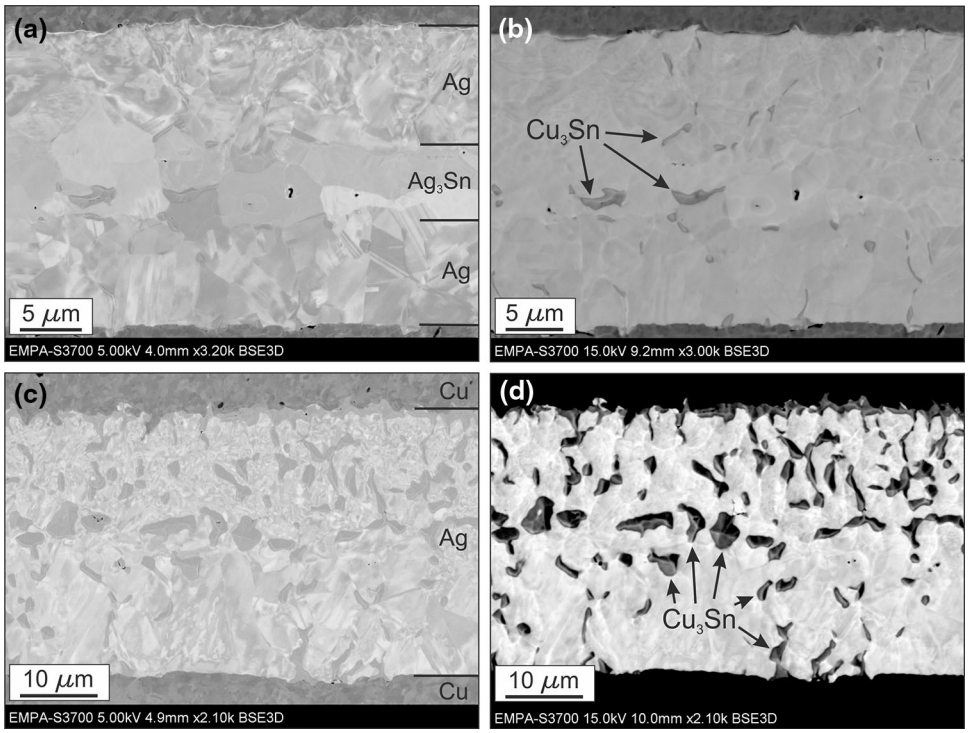

Fig. 4. TLP bonded microstructure with Ag–Ag_3Sn–Ag during annealing at 300°C, as grain structure image after (a) 400 h and (c) 1200 h, and as phase-contrast image after (b) 400 h and (d) 1200 h.

defects appear in the central part of the TLP-bonded samples, as is apparent in Fig. 5c.

A mean shear strength of 27.4 ± 6.4 MPa was measured for samples bonded at 300°C, i.e. significantly lower than for samples A. The fracture surface shown in Fig. 6 confirms that the failure behavior is purely brittle and occurs within the Ni_3Sn_4 IMC layer at one of the defect planes. Needle-like IMC structures can be detected, with regularly distributed holes which represent the pores already viewed during the investigation of microstructure (Fig. 5b).

Phase Formation During Annealing

Samples B for annealing experiments with Ni–Ni_3Sn_4–Ni interlayers were TLP-bonded at 300°C for 60 min; the microstructure is shown in Fig. 5b. At 200°C, no changes of the microstructure could be observed after isothermal annealing for up to 1200 h.

When the annealing temperature was increased to 300°C, formation of a Ni_3Sn_2 layer 1 μm thick was observed at the initial Ni–Ni_3Sn_4 interface after 400 h of holding time. This is in agreement with the Ni–Sn binary phase diagram which predicts the Ni_3Sn_2 phase when moving from the Sn-rich side toward the Ni-rich side. The microstructure of these samples is shown in Fig. 7a, in which a slight BSE contrast between Ni_3Sn_4 and Ni_3Sn_2 is visible. The defect size and amount is remarkably reduced compared with the as-bonded samples (Fig. 4b). Therefore, submicron-sized pores appear at the Ni–Ni_3Sn_2 interface.

With a longer annealing time of 1200 h, the thickness of the Ni_3Sn_2 layers approximately doubles and reaches a mean value of 2 μm. Simultaneously, Ni_3Sn layers of averaged thickness 0.75 μm form at the initial Ni–Ni_3Sn_2 interfaces. Although the Ni_3Sn layer grows more slowly than the Ni_3Sn_2 layer, Ni atoms can still diffuse into Ni_3Sn_2 and the system tends to form the final IMC phase in accordance with the binary Ni–Sn phase diagram. The corresponding microstructure is shown in Fig. 7b, in which the single layers are distinguished by adjustment of the BSE phase contrast. Pore size and the number of pores in the IMC layer are slightly reduced compared with the samples annealed for 400 h. The electroplated Ni layer acts as an effective diffusion barrier for Cu atoms from the substrate material under these experimental conditions, because Cu–Sn IMC did not appear and Cu was not detected anywhere in the interlayer system (in contrast with samples A with Ag layers, as discussed in the section "Phase Formation During Annealing").

TLP Bonding with Ag–Sn–Ni Combined Interlayers

Phase Formation During TLP Bonding

As is apparent from Fig. 8a and b, holding isothermal at 260°C for 80 min was not sufficient to

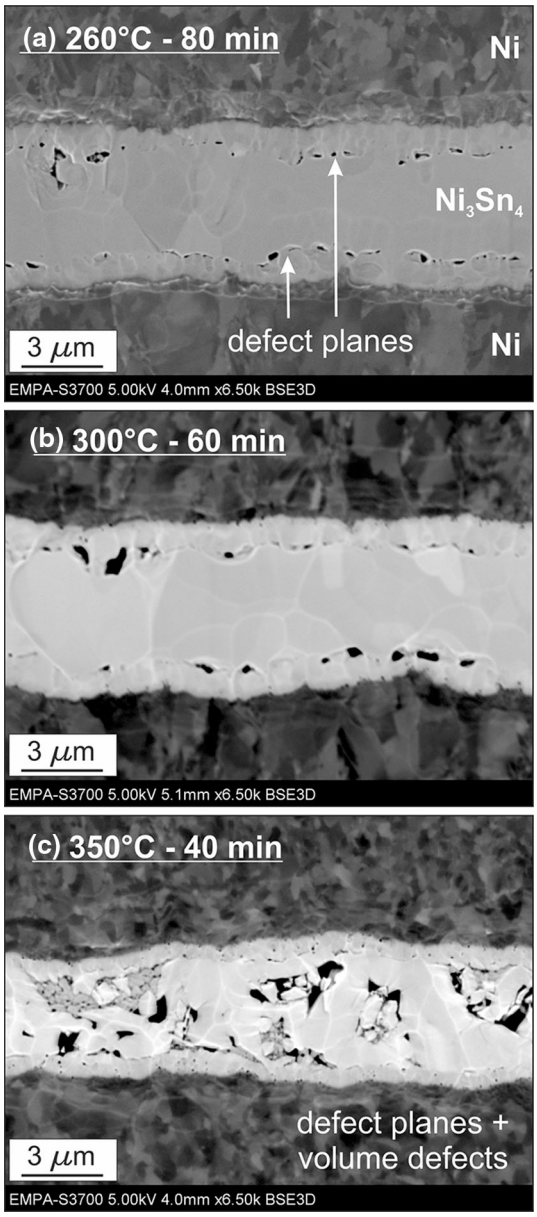

Fig. 5. TLP bonding of samples B at (a) 260°C, (b) 300°C, and (c) 350°C.

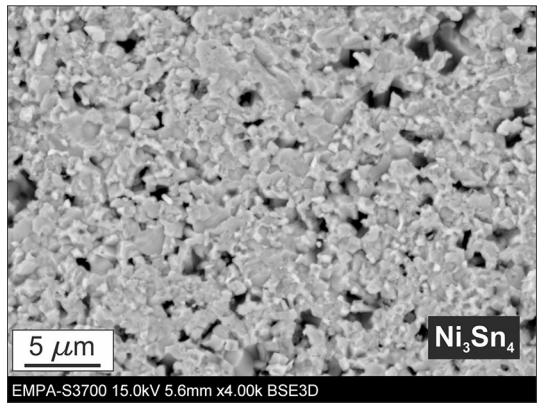

Fig. 6. Top view on fracture surface of samples B.

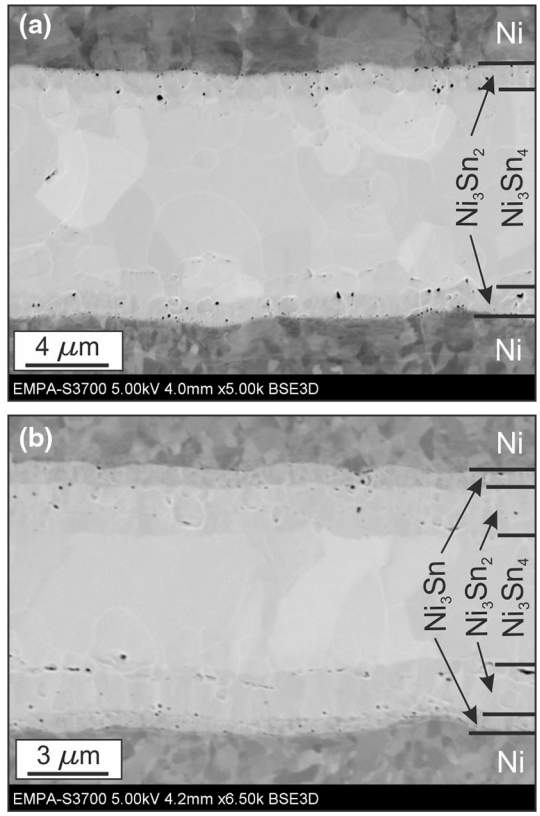

Fig. 7. TLP bonded microstructure with Ni–Sn–Ni after annealing at 300°C for (a) 400 h and (b) 1200 h.

completely transform the liquid Sn layer into IMC, although complete transformation was expected according to Eq. 1. Characteristic features of Ag_3Sn and Ni_3Sn_4 IMC morphology can be seen: the Ni_3Sn_4 IMC layer at the Ni interface grows with elongated and faceted structures whereas the Ag_3Sn phase forms scallop-like IMC. Ni_3Sn_4 IMC islands are embedded in the remaining Sn and detached from the needle-shaped IMC layer below. It can be remarked that these IMC islands hinder growth of Ag_3Sn scallops, as indicated at Pos. 1 and Pos. 2. The scallops are forced to grow around the Ni_3Sn_4 IMC islands; this results in a change of their well-defined scallop-like shape.

When the process temperature is increased to 300°C, an intermetallic bonding zone with a very small number of defects is obtained, as shown in Fig. 8c and d. Valleys between single Ni_3Sn_4 needles are filled with Ag_3Sn IMC. Small amounts of small submicron-sized defects can be observed within the Ni_3Sn_4 layer only.

However, further increase of the process temperature to 350°C clearly results in more defects, as illustrated in Fig. 8e and f. Pores of size of up to 2 μm form predominantly within the Ni_3Sn_4 layer; a

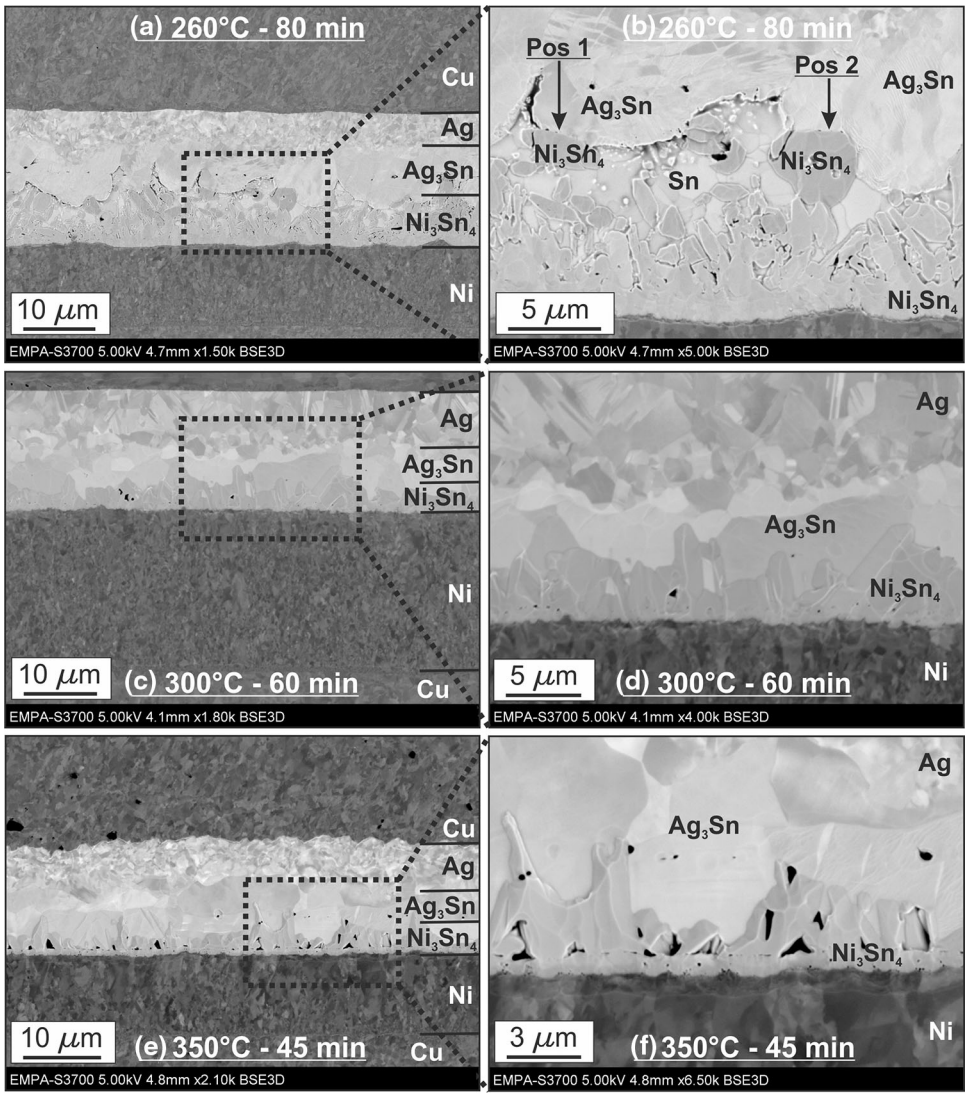

Fig. 8. TLP bonding of samples C at (a) 260°C, (c) 300°C, (e) 350°C, and, with higher magnification, in (b), (d), and (f).

smaller amount of smaller pores of size <1 μm occurs within the Ag_3Sn IMC layer.

Shear tests on samples C, TLP bonded at 300° C, resulted in a mean shear strength of 40.7 ± 13.7 MPa. The brittle fracture behavior is dominated by the Ni_3Sn_4 IMC, and crack propagation mainly occurs within the Ni_3Sn_4 layer, where pores are mainly expected. However, the fracture surface in Fig. 9 also shows that failure can occur along the Ag_3Sn–Ni_3Sn_4 interface when Ag_3Sn scallops are visible. The shear strength is between those obtained for samples A and B. Although failure appears in the Ni_3Sn_4 layer for samples B and C (predominantly), the much smaller number of defects in samples C leads to the increase of shear strength.

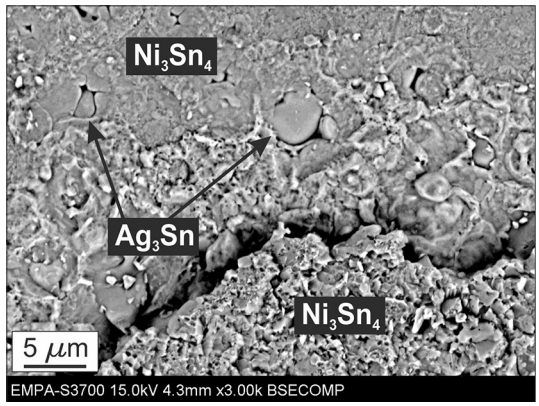

Fig. 9. Top view on fracture surface of samples C.

Phase Formation During Annealing

Annealing experiments were conducted on samples C with combined IMC layers Ag–Ag_3Sn–Ni_3Sn_4–Ni which were TLP bonded at 300°C for 60 min, on the basis of investigations reported in the section "Phase Formation During TLP

Bonding". Changes in microstructure were monitored during annealing at 200°C when, after 400 h, Ag_3Sn IMC was already transformed into Ag–Sn solid solution and a more or less planar layer of Ni_3Sn_4 formed. The Ag layer contained 6 at.% Sn. Interestingly, the microstructure did not change further when the samples were annealed for 1200 h, as shown in Fig. 10a

Annealing at 300°C for 400 h led to formation of $(Ni,Cu)_3Sn$ IMC containing 55 at.% Ni, 12 at.% Cu, and 33 at.% Sn. Cu was again provided by diffusion from the substrate through the Ag layer. Ag_3Sn IMC was not found in the joint. Longer annealing time up to 1200 h did not further affect the microstructure and the chemical phase composition within the samples, as illustrated in Fig. 10b. However, the transformations at 300°C were accompanied by formation of pores within the IMC layer and at the $(Ni,Cu)_3Sn$–Ni and $(Ni,Cu)_3Sn$–Ag interfaces.

DISCUSSION

Mechanisms of Defect Formation During TLP Bonding

TLP bonding of samples A, B, and C with different interlayer combinations revealed that the process temperature has a significant effect on the microstructure of the joint, in particular the number, size, and position of pores. Irrespective of the interlayer system, an ideal process temperature of approximately 300°C was identified. At this temperature the number of pores was minimized and the reaction kinetics were maximized, resulting in the most efficient joining process.

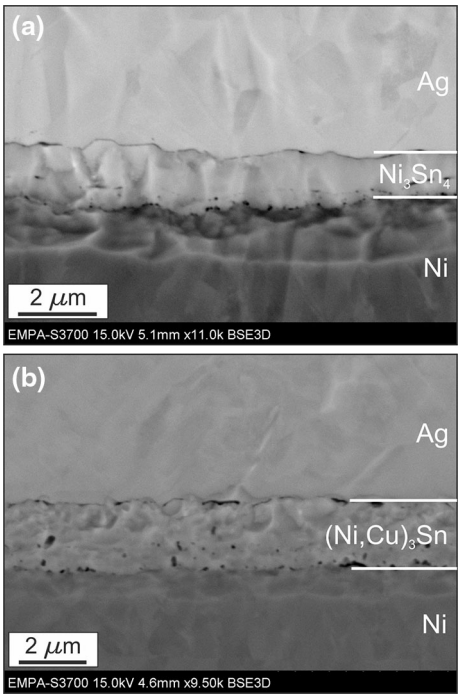

Fig. 10. TLP bonded microstructure with Ag–Ag_3Sn–Ni_3Sn_4–Ni after annealing for 1200 h at (a) 200°C and (b) 300°C.

In our previous work on the formation of Ag_3Sn IMC,[15] we proved that the root-mean-square (RMS) roughness of the scallop-like Ag_3Sn IMC growing toward the liquid Sn phase increases with higher holding temperature. Scallops become broader and more irregular. During TLP bonding, scallops symmetrically nucleate at both Ag–Sn interfaces and propagate into the liquid Sn. After a specific time, both growth front lines meet and leave behind entrapped Sn islands in the center of the joint which are isothermally transformed into Ag_3Sn IMC. Equation 4 shows the reactions from incomplete to complete IMC transformation:

$$3Ag + Sn + Ag_3Sn \rightarrow 2Ag_3Sn \Rightarrow 3Ag + Sn \rightarrow Ag_3Sn \quad (4)$$

When mass conservation is considered, the volume difference ΔV between IMC and base materials can be obtained from:

$$\Delta V = 1 - \frac{1M(Ag_3Sn)/\rho(Ag_3Sn)}{3M(Ag)/\rho(Ag) + 1M(Sn)/\rho(Sn)} \quad (5)$$

According to Eq. 5, the transformation process leads to volume contraction of approximately 9 vol.% and the probability of shrinkage porosity is expected to increase when the remaining Sn islands are large. Because of the temperature-dependent morphology of the Ag_3Sn scallops, the size of the Sn islands will increase when higher process temperatures are used. The process of defect formation during TLP bonding with Ag–Sn–Ag interlayers is shown schematically for a process temperature T_1 in Fig. 11a and b and for T_2 ($>T_1$) in Fig. 11c and d. This model is in good agreement with the experimental observations in Fig. 2, when massive scallops grew at 350°C after 1 min (Fig. 2c) whereas more but smaller scallops nucleated at 300°C after 1 min (Fig. 2a). Higher process temperature resulted in a flawed TLP joint (Fig. 2d), and reducing the temperature by 50°C led to only sporadic development of submicron-sized pores (Fig. 2b). As predicted by the model, pores form within the Ag_3Sn IMC layer in which scallops growing from both sides impinge.

The model for formation of shrinkage porosity in samples A was further confirmed by means of an additional TLP experiment at 320°C with a dwell time of 20 min. Figure 12 shows the microstructure of this joint when the TLP process is incomplete, yet as it could be estimated by use of Eq. 1. At this late reaction stage, randomly distributed Sn entrapments can be seen within the IMC layer. The magnified view of one of these Sn islands in Fig. 12b reveals that pores can form as a result of different specific volumes of Sn and Ag_3Sn. Bosco's model[31] of defect formation during TLP bonding with Cu–Sn–Cu interlayers cannot be used for our joining con-

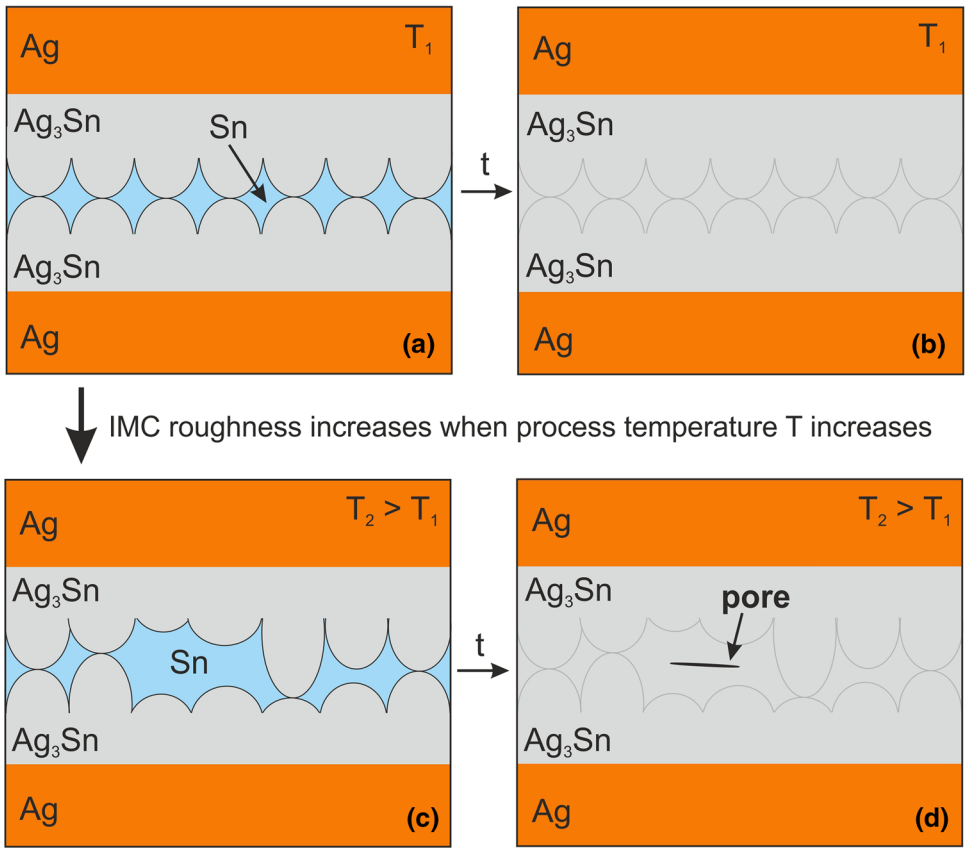

Fig. 11. Schematic diagram of TLP bonding by use of Ag–Sn–Ag interlayers, with intermediate step and after full transformation into IMC at T_1 in (a) and (b) and at $T_2 > T_1$ in (c) and (d).

figuration, because the issue of solid-state IMC formation was effectively bypassed by using Sn foil instead of coatings. Bosco identified Sn coating thickness and heating rate as crucial factors, and our work extends this concept and introduces process temperature as having a major effect on the microstructure of TLP bonded joints.

The porosity of TLP bonded samples B with Ni–Sn–Ni interlayers can be deduced from a volume contraction of approximately 11 vol.% when Eqs. 4 and 5 are applied to Ni_3Sn_4 IMC formation. This is in good agreement with the value obtained in Ref. 34 when void formation in the Ni–Sn system under solid-state conditions was correlated with shrinkage effects. At processing temperatures of 260°C and 300°C, pores only appear in two defect planes at a defined distance from the Ni layers. This effect is a result of the morphological characteristics of Ni_3Sn_4 IMC growth.[8,9,36] After nucleation, needle-like Ni_3Sn_4 IMC grains grow from the liquid, as shown in Fig. 13a. Ni can dissolve in the liquid Sn, because the IMC layer is not dense and intimate contact points between Ni and liquid Sn provide fast diffusion paths. Because of needle growth in the length and width directions, the IMC layer at the Ni interface densifies and becomes detached, and more or less equiaxed Ni_3Sn_4 IMC particles nucleate within the liquid Sn, as shown schematically in Fig. 13b. Persistent diffusion of Ni into the liquid Sn through the Ni_3Sn_4 IMC layer leads to coalescence of the Ni_3Sn_4 particles, and Sn islands form ahead of the needle-like IMC. Shrinkage porosity occurs and leaves defect planes behind, as observed experimentally. The final process step, with full transformation into the IMC, is shown schematically in Fig. 13c. At 350°C, large defects also appear along the center of the joint, probably because of very irregular growth of the detached Ni_3Sn_4 particles and formation of Sn entrapments. The number of pores in samples B could be reduced by choosing a process temperatures below 300°C but (nearly) defect free TLP joints could not be achieved, in contrast with samples A. Growth of detached Ni_3Sn_4 IMC can certainly be avoided by using much thinner Sn foil (approx. 2 μm). Handling of such thin foil is, however, very difficult.

In contrast with samples A and B, for which a lower process temperature led to better joints, a narrow temperature range at approximately 300°C was identified for samples C with combined layers of Ag–Sn–Ni in which a nearly defect-free microstructure was obtained. Ag_3Sn IMC fill the valleys of Ni_3Sn_4 needles, as is apparent in Fig. 8c and d. Formation of two neighboring IMC layers is different from the morphology suggested in the patent by Chang,[35] in which the second intermetallic phase is

supposed to be fully integrated within the first intermetallic phase. Single small pores can be found only within the Ni_3Sn_4 layer. At 350°C, the position of most of the pores is identical but their size and number increase substantially because of more irregular growth of the IMC needles and shrinkage porosity (Fig. 6e and f). At a lower temperature, 260°C, process kinetics, of the Ag_3Sn IMC scallops in particular, are too slow to meet the Ni_3Sn_4 IMC needles before the detached Ni_3Sn_4 particles nucleate as shown in Fig. 13. These particles act as obstacles to the scallops, as indicated by Pos. 1 and 2 in Fig. 8b. Consequently, after 80 min dwell time (sufficient when kinetics for the individual systems Ag–Sn and Ni–Sn are considered), a large volume of Sn is still left in the system. Besides very slow kinetics, the TLP joint is expected to result in a large number of defects after full transformation into IMC. It is essential for homogeneous and defect-free TLP joints to have a second intermetallic phase, here Ag_3Sn, with sufficiently rapid kinetics to prevent the detached Ni_3Sn_4 IMC from nucleation.

In general, the volume of the entrapped Sn islands is related to coarsening and the interfacial roughness (i.e. irregularity) of the IMC forming within the liquid Sn layer. Because both increase with increasing temperature and time, the process can be adjusted to achieve void reduction. In this study the threshold value for temperature was found experimentally to be 300°C, but it can be strongly assumed that thinner Sn foil (faster process time) will also lead to fewer defects within the IMC layer.

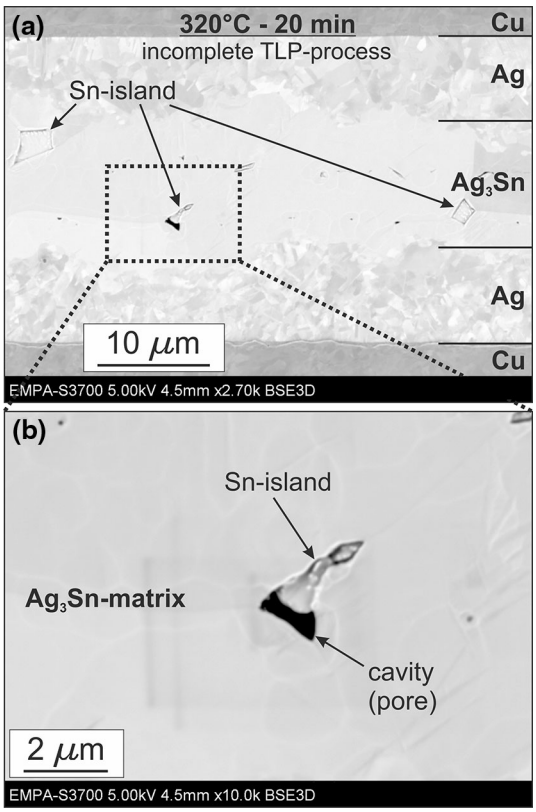

Fig. 12. (a) Entrapped Sn islands after incomplete TLP process with Ag–Sn–Ag interlayers, (b) pore formation from Sn island.

Thermal Stability of TLP-Bonded Microstructures

As documented by Bosco et al.[32] and Gollas et al.,[33] TLP bonded systems tend to transform toward phases with a higher proportion of the high-melting-point material, i.e. Ag, Ni, or Cu, and finally into solid solution during heat treatment. Our work showed that the required mobility of atoms is not sufficiently high at 200°C and the microstructures hardly change in binary interlayer systems after long-term annealing up to 1200 h. Thus, TLP bonding is a promising technique for chip packaging

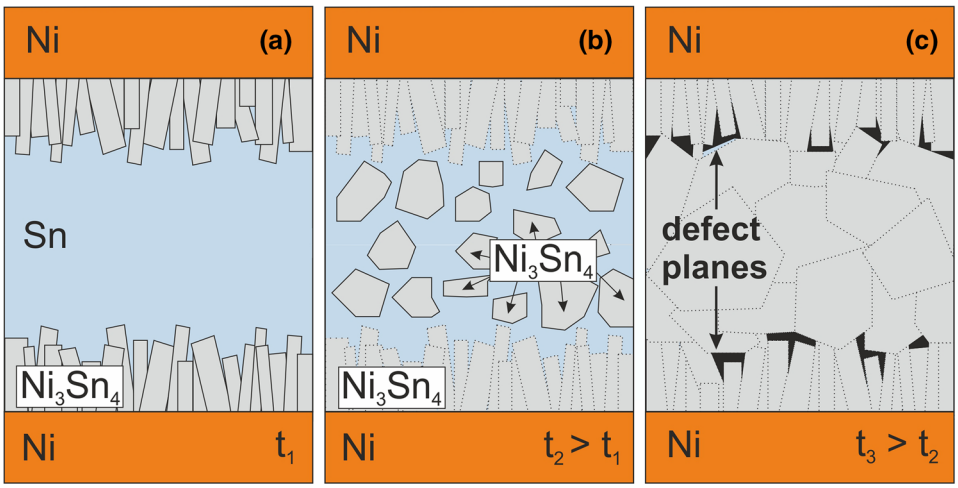

Fig. 13. Schematic diagram of TLP bonding using Ni–Sn–Ni interlayers: (a) early stage after t_1, (b) intermediate stage after $t_2 > t_1$ and (c) after full transformation into IMC after $t_3 > t_2$.

applications when peak temperatures up to 175°C are applied. Because the microstructure is stable, mechanical, thermal, and electrical properties will not change during operation (unless as a result of thermo-mechanical fatigue). In combined interlayers with adjacent Ag_3Sn and Ni_3Sn_4 IMC, transformations are driven toward Ni_3Sn_4 IMC, as a result of the different enthalpy of formation, ΔH_f. Ni_3Sn_4 IMC are energetically favored with $\Delta H_f = -7.4$ kJ/mol$_{Sn}$[37] compared with Ag_3Sn with $\Delta H_f = -4.2$ kJ/mol$_{Sn}$.[38] When transformation into a planar Ni_3Sn_4 layer is complete after 400 h, the microstructure does not further change during long-term annealing. The remelting temperature of the joint is increased from 480°C (T_{m,Ag_3Sn}) in the as-bonded state to 794.5°C (T_{m,Ni_3Sn_4}) after annealing.

Annealing at 300°C can be used to adjust the characteristics of the microstructure of TLP-bonded components and to improve the properties of the joint. For samples A, two transformation processes overlap when the Ag_3Sn IMC is converted into an Ag–Sn solid solution and Cu_3Sn particles form because of diffusion of Cu from the substrate material into the TLP system. Elongated Cu_3Sn precipitates evolve randomly within the Ag_3Sn IMC layer and the Ag–Sn solution along grain boundaries where Cu diffuses fastest. Cu_3Sn IMC are energetically favored with a enthalpy of formation $\Delta H_f = -8.2$ kJ/mol$_{Sn}$ compared with the Ag_3Sn IMC with $\Delta H_f = -4.2$ kJ/mol$_{Sn}$.[38] Because Ag_3Sn IMC and Cu_3Sn both have an orthorhombic structure, Cu atoms can easily substitute Ag atoms in the crystal lattice. This effect could be avoided by depositing diffusion barriers consisting of, e.g., Ni or W between the Cu substrate and the Ag coating. After long-term annealing for 1200 h, the transformation processes result in a microstructure of Cu_3Sn particles embedded in a matrix of Ag–Sn solid-solution, as shown in Fig. 4. It is important to mention that the initial interlayer thickness ratio of Ag/Sn (3.5/1) was not sufficient to form Ag–Sn solid solution, which requires a ratio of at least 5.7/1, so full transformation into Ag–Sn solid solution was only enabled by simultaneous formation of Cu_3Sn. Because of the lack of Ag, transformation into the Ag–Sn solid solution requires much more time than reported by Gollas et al.,[33] when 480 min at 320°C were sufficient. The remelting temperature of the joint is increased and limited by the melting point of Cu_3Sn (676°C). It can be assumed that the thermal, electrical, and possibly mechanical properties of the joint are enhanced. Bosco et al.[32] reported an increase of bending strength from 300 MPa to 400 MPa when they compared TLP bonded joints consisting of only Cu–Sn IMC with a mixture of solid solution and IMC. However, this aspect might be subject of a follow-up project because this work focused mainly on microstructure.

Microstructure changes were also monitored for samples B with initial Ni–Ni_3Sn_4-Ni interlayers. The transformations were in accordance with the binary Ni–Sn phase diagram, driven in the direction of the lowest enthalpy of formation when the Ni_3Sn_4 phase ($\Delta H_f = -7.4$ kJ/mol$_{Sn}$) is converted into Ni_3Sn_2 ($\Delta H_f = -17.5$ kJ/mol$_{Sn}$) and subsequently into Ni_3Sn ($\Delta H_f = -21$ kJ/mol$_{Sn}$).[37] The phase transformations depend on diffusion of Ni into the Ni–Sn IMC; at 300°C this is too slow for full transformation into the final Ni_3Sn phase after 1200 h. A layered structure consisting of Ni_3Sn ($T_{m,Ni_3Sn} = 1174$°C), Ni_3Sn_2 ($T_{m,Ni_3Sn_2} = 1264$°C) and Ni_3Sn_4 ($T_{m,Ni_3Sn_4} = 794.5$°C) was obtained after annealing for 1200 h, as shown in Fig. 7b, because in the Ni–Sn system solubility of Sn atoms in the Ni lattice is only very low. Partial phase transformations within the TLP joint occur in the volume where pores are formed after TLP bonding. After transformation, the size of these pores is substantially reduced which can be related to volume expansion of 6 vol.% for $Ni_3Sn_4 \rightarrow Ni_3Sn_2$ and 3 vol.% for $Ni_3Sn_2 \rightarrow Ni_3Sn$. This expansion works opposite to the volume contraction described in the section "Mechanisms for Defect Formation During TLP Bonding", which accounts for shrinkage porosity during TLP bonding. The Ni coating effectively prevented Cu from diffusion into the TLP joint.

Annealing of combined interlayers is affected by diffusion of Cu through the Ag layer so that intermixing leads to formation of $(Ni,Cu)_3Sn$ IMC after 400 h. Because no further changes of the microstructure were observed during long-term annealing up to 1200 h, it can be assumed that the configuration is stable against service temperatures of 300°C. Slight degradation of the microstructure was observed for samples C annealed at 300°C when the transformations led to formation of pores within the IMC layer and between IMC and base metallization, which may weaken the structural integrity of these joints. It is noteworthy that formation of $(Ni,Cu)_3Sn$ IMC and possibly pores could be suppressed by use of diffusion barriers between the Cu substrate and the Ag coating. Observations of phase transformations during annealing in this work might be useful for the studies reported in Refs. 34 and 35 with TLP joints consisting of different IMC in intimate contact.

CONCLUSIONS

This work chose an approach in which Cu substrates were TLP bonded with Ag–Sn–Ag, Ni–Sn–Ni, and combined Ag–Sn–Ni interlayers. Because the CTE mismatch was kept low, characteristics of the TLP process and the mechanical and thermal behavior of TLP bonded components could be investigated without significant interference from thermally induced residual stresses. The following scientific conclusions were derived.

1. The optimum process temperature was 300°C for all three interlayer systems; at this temperature the number of pores is minimized and the process efficiency (IMC growth rate) is high.

2. It was verified experimentally that the mechanisms of pore formation were related to volume contraction (shrinkage porosity) during isothermal solidification from liquid Sn into IMC. Different defect positions and amounts were ascribed to the specific IMC growth characteristics of each interlayer system.
3. Mechanical shear strength was shown to be highest for samples A (Ag–Ag_3Sn–Ag) and C (Ag–Ag_3Sn–Ni_3Sn_4–Ni), 60.4 MPa and 40.7 MPa, respectively, and lowest for samples B (Ni–Ni_3Sn_4–Ni), 27.4 MPa. Crack propagation occurred within the IMC layer where pores weaken the structural integrity. Ductile fracture features were identified within Ag_3Sn IMC whereas Ni_3Sn_4 IMC fracture was purely brittle.
4. Long-term annealing at 200°C resulted in binary TLP bonded systems with very good microstructure stability. At 300°C, IMC phases transform toward Ag–Sn solid solution (from Ag_3Sn) and Ni_3Sn (from Ni_3Sn_4). Cu diffuses into Ag along grain boundaries and forms regularly distributed Cu_3Sn precipitates. Combined IMC interlayers in samples C transform toward Ni-based IMC at 200°C and 300°C. Ag–Sn–Ag and Ni–Sn–Ni TLP systems are suitable for service temperatures up to 300°C without any degradation of microstructure. Combined interlayers with the Ag–Sn–Ni stacking sequence are recommended for service up to 200°C, because pore formation occurs during annealing at 300°C.

ACKNOWLEDGEMENT

The authors gratefully acknowledge ABB Corporate Research Switzerland for financing this study and, in particular, Dr. Slavo Kicin for his support.

REFERENCES

1. B.J. Baliga, *IEEE Electr. Device L.* 10, 455 (1989).
2. M. Willander, M. Friesel, Q.U. Wahab, and B. Straumal, *J. Mater. Sci.* 17, 1 (2006).
3. G.O. Cook and C.D. Sorensen, *J. Mater. Sci.* 46, 5305 (2011).
4. R. Labie, W. Ruythooren, and J. Van Humbeeck, *Intermetallics* 15, 396 (2007).
5. M.S. Park and R. Arroyave, *Acta Mater.* 58, 4900 (2010).
6. M. Schaefer, R.A. Fournelle, and J. Liang, *J. Electron. Mater.* 27, 1167 (1998).
7. A.C.K. So, Y.C. Chan, and J.K.L. Lai, *IEEE T. Compon. Pack B* 20, 161 (1997).
8. S. Bader, W. Gust, and H. Hieber, *Acta Metall. Mater.* 43, 329 (1995).
9. J. Gorlich, D. Baither, and G. Schmitz, *Acta Mater.* 58, 3187 (2010).
10. D. Gur and M. Bamberger, *Acta Mater.* 46, 4917 (1998).
11. Y.W. Lin and K.L. Lin, *J. Appl. Phys.* 108, 063536 (2010).
12. J.O. Suh, K.N. Tu, A.T. Wu, and N. Tamura, *J. Appl. Phys.* 109, 123513 (2011).
13. M.L. Huang, F. Yang, N. Zhao, and Y.C. Yang, *J. Alloy. Compd.* 602, 281 (2014).
14. J.F. Li, P.A. Agyakwa, and C.M. Johnson, *Acta Mater.* 58, 3429 (2010).
15. A. Lis, M.S. Park, R. Arroyave, and C. Leinenbach, *J. Alloy. Compd.* 617, 763 (2014).
16. Z. Marinkovic and V. Simic, *Thin Solid Films* 195, 127 (1991).
17. S.K. Sen, A. Ghorai, A.K. Bandyopadhyay, and S. Sen, *Thin Solid Films* 155, 243 (1987).
18. K. Suzuki, S. Kano, M. Kajihara, N. Kurokawa, and K. Sakamoto, *Mater. Trans.* 46, 969 (2005).
19. J.C. Lin, L.W. Huang, G.Y. Jang, and S.L. Lee, *Thin Solid Films* 410, 212 (2002).
20. Y.M. Liu, Y.L. Chen, and T.H. Chuang, *J. Electron. Mater.* 29, 1047 (2000).
21. Y.M. Liu and T.H. Chuang, *J. Electron. Mater.* 29, 405 (2000).
22. M. Millares, B. Pieraggi, and E. Lelievre, *Scripta Metall. Mater.* 27, 1777 (1992).
23. R. Roy and S.K. Sen, *Thin Solid Films* 197, 303 (1991).
24. J.S. Kim, T. Yokozuka, and C.C. Lee, *Mat. Sci. Eng. A-Struct.* 458, 116 (2007).
25. J.F. Li, P.A. Agyakwa, and C.M. Johnson, *J. Electron. Mater.* 43, 983 (2014).
26. P.J. Wang, J.S. Kim, and C.C. Lee, in *12th IEEE International Symposium on Advanced Packaging Materials: Processes, Properties, and Interface* (2007). doi:10.1109/ISAPM.2007.4419926.
27. T. Takahashi, S. Komatsu, and T. Kono, *Electrochem. Solid St.* 12, H263 (2009).
28. T.A. Tollefsen, A. Larsson, M.M.V. Taklo, A. Neels, X. Maeder, K. Hoydalsvik, D.W. Breiby, and K. Aasmundtveit, *Metall. Mater. Trans. B* 44, 406 (2013).
29. S.H. Eo, D.S. Kim, H.J. Jeong, and J.H. Jang, *Electron. Mater. Lett.* 9, 787 (2013).
30. B. Grummel, H.A. Mustain, Z.J. Shen, and A.R. Hefner, *Proc. Int. Symp. Power* (2011) 260.
31. N.S. Bosco and F.W. Zok, *Acta Mater.* 52, 2965 (2004).
32. N.S. Bosco and F.W. Zok, *Acta Mater.* 53, 2019 (2005).
33. B. Gollas, J.H. Albering, K. Schmut, V. Pointner, R. Herber, and J. Etzkorn, *Intermetallics* 16, 962 (2008).
34. H.Y. Chuang, J.J. Yu, M.S. Kuo, H.M. Tong, and C.R. Kao, *Scripta Mater.* 66, 171 (2012).
35. J.Y. Chang, T.C. Chang, T.H. Chuang, and C.Y. Lee, Dual-phase intermetallic interconnection structure and method of fabricating the same, US Patent, US8742600B2, 2014.
36. A. Lis, C. Kenel, and C. Leinenbach, Empa - Swiss Federal Laboratories for Materials Science and Technology, CH-8600 Duebendorf, submitted for publication (2015).
37. G.P. Vassilev, K.I. Lilova, and J.C. Gachon, *Thermochim. Acta* 447, 106 (2006).
38. H. Flandorfer, U. Saeed, C. Luef, A. Sabbar, and H. Ipser, *Thermochim. Acta* 459, 34 (2007).